J. Biochem. 2010;147(4):555–563 doi:10.1093/jb/mvp201

JB THE JOURNAL OF BIOCHEMISTRY

Image analysis of α/β-tubulin rings in two-dimensional crystalline arrays of periodic mesoporous nanostructures

Received November 12, 2009; accepted November 26, 2009; published online December 2, 2009

Noriyuki Ishii[1,*], Kou Okuro[2], Kazushi Kinbara[3] and Takuzo Aida[2,4]

[1]Institute for Biological Resources and Functions, National Institute of Advanced Industrial Science and Technology (AIST), Central-6, 1-1-1 Higashi, Tsukuba-shi, Ibaraki 305-8566, [2]Department of Chemistry and Biotechnology, School of Engineering, The University of Tokyo, 7-3-1 Hongo, Bunkyo-ku, Tokyo 113-8656, [3]Institute of Multidisciplinary Research for Advanced Materials, Tohoku University, 2-1-1 Katahira, Aoba-ku, Sendai-shi, Miyagi 980-8577 and [4]ERATO-SORST Nanospace Project, Japan Science and Technology Agency (JST), National Museum of Emerging Science and Innovation, 2-41 Aomi, Koto-ku, Tokyo 135-0064, Japan

*Noriyuki Ishii, Institute for Biological Resources and Functions, National Institute of Advanced Industrial Science and Technology (*AIST*), Central-6, 1-1-1 Higashi, Tsukuba-shi, Ibaraki 305-8566, Japan, Tel.: +81 29 861 6119, Fax: +81 29 861 6123, E-mail: ishii@ni.aist.go.jp

Two-dimensional crystalline arrays of periodic mesoporous nanostructures, consisting of α/β-tubulin ring-shaped oligomers in the double-layered architecture in an apolar arrangement are successfully prepared with PEM-G buffer containing Arginine nonamers and observed by electron microscopy. The ring-shaped α/β-tubulin assemblies are conformations related to a protofilament, although protofilaments are usually highly constrained in a straight conformation in microtubules. The two-dimensional crystalline arrays appear to have the structure of a square lattice with the layer group *P*4, the unit cell dimensions of $a = b = 36.9$ nm and $\gamma = 90^\circ$. The isolated torus-like shaped projections of a pseudo-repeat structural unit are analysed with the method for single particle reconstruction. The average values of outer- and inner-diameters for the torus-like shapes are 49.0 ± 1.0, and 25.4 ± 1.1 nm, respectively. The thickness of the peripheral masses consisting of two concentric sub-rings is 11.8 ± 1.0 nm, where α/β-tubulin heterodimers appear to reside alternately. Taking the average sizes of the rings and the crystallographic unit cell dimensions into consideration, the discussion is focused on the most probable arrangement of the α/β-tubulin rings in the two-dimensional crystalline arrays.

Keywords: Two-dimensional crystals/α/β-tubulin ring/electron microscopy.

Abbreviations: Arg_9, arginine nonamer trifluoroacetate salt; EGTA, ethylene glycol tetraacetic acid; GDP, guanosine diphosphate; GTP, guanosine triphosphate; SDS-PAGE, sodium dodecyl sulphate-polyacrylamide gel electrophoresis; TEM, transmission electron microscopy.

Microtubules are one of the components of the cytoskeleton, which mediate cellular functions, including vesicular transport to cell motility and mitosis (*1*). Owing to their fundamental role during mitosis, microtubules have been a target for the development of anti-mitotic drugs, which interfere with microtubule dynamics, such as paclitaxel and its derivatives (*2*, *3*). The microtubules have a diameter of 25 nm and length varying from 200 nm to 25 μm. In microtubules, repeating α/β-tubulin heterodimers that bind head to tail assemble into a protofilament (*4*). The protofilaments are arranged side by side in a cylindrical arrangement forming a microtubule. It is widely considered that microtubules can have a range of protofilament numbers. The main components of microtubules, α- and β-tubulin each have molecular masses of 55 kDa. These subunits are slightly acidic with an isoelectric point between 5.2 and 5.8. Tubulin is a guanosine triphosphate (GTP)-binding protein and both α- and β-tubulin bind one GTP. The binding is non-exchangeable in α-tubulin, but it is exchangeable in β-tubulin.

Tubulin adopts several different conformations and this conformational flexibility is generally believed to be the basis for its different functions in the cell. Polymerization of tubulin into microtubules is a self-assembly process and whole information necessary for forming the final structure is filled in each subunit. Microtubules can switch between growing and shrinking phase in a process known as dynamic instability and is related to GTP hydrolysis in β-tubulin. Dynamic instability is precisely regulated during cell cycle by microtubule-associated proteins through cascades of phosphorylation–dephosphorylation events (*5*). Thus, it takes place during microtubular assembly through the hydrolysis of the GTP bound to β-tubulin molecule. The hydrolysis occurs during the polymerization into microtubule; therefore, a resultant microtubule assembly is composed of guanosine diphosphate (GDP)-liganded β-tubulin subunits. According to the currently prevailing scenarios for polymerization and depolymerization, together with the α/β-tubulin structure determined from cryo-EM three-dimensional reconstruction (*6*) as well as X-ray crystallography (*7*), β-tubulin subunit bound GDP form is unfavourable for polymerization. The conformational tension accumulates so long as the subunits are within the microtubule lattice. The GTP cap model along with the high-resolution molecular structures suggests that the microtubule is stabilized by a layer of GTP-liganded subunits at the end edges. When GTP cap is removed, depolymerization occurs rapidly.

Based on the observations of protofilaments peeling off from the end portion of depolymerizing microtubules, these curved protofilaments will further break down to dimers that are capable of exchanging GDP for GTP and then become ready for another turn of polymerization. There is a greater tendency of GDP-liganded tubulin to form ring structure of polymers compared with GTP-liganded tubulin. Therefore, tubulin can exist in two different conformations, a GDP-liganded conformation, which prefers to form curved protofilaments unable to polymerize into microtubules, and a GTP-liganded conformation, which tends to form straight protofilaments amenable for polymerization into microtubules. In the microtubule lattice, GDP-liganded tubulin adopts a conformation similar to GTP-liganded conformation, thus conformational strain appears to increase because of hydrolysis.

The structure of α/β-tubulin heterodimer determined from the electron crystallography using the zinc-induced sheets (*3*, *6*) has provided some insights into explaining polymerization-induced hydrolysis; however, it appears that static crystallographic structures can not be used to address the question of how this hydrolysis may link to depolymerization. The curvature of a depolymerizing, GDP-liganded tubulin containing protofilament may be dominant due to the weakening and bending of the longitudinal contact at the dimer interfaces where the hydrolyzed nucleotide resides and a conformational change occurring in the subunit may further facilitate the events. Although the relationship between the hydrolysis and depolymerization at the end of microtubules has been studied by several groups to explain the relation between these local dynamics and large-scale structure formation (*8–11*), it is not yet conclusive, especially with regard to the formation of a crystalline structure. On the contrary, an alternate interpretation has been reported from theoretical calculation based on electron microscopy (EM) imaging. The authors have proposed that GTP-liganded conformation is also curved and that the binding of the nucleotide primarily involves the strength of lateral interactions (*12–14*).

The curved conformations of protofilaments where GDP-liganded tubulin reside are stabilized by high concentration of magnesium and other divalent ions. In turn, GDP-liganded tubulin dimers polymerize into curved protofilaments in the presence of these divalent cations and often close into ring structures (*15*, *16*). Ring structures of GDP-liganded tubulin have been observed in many characteristic variations, including the predominant forms in the presence of divalent cations reported by Nicholson *et al.* (*17*). Mono-dispersed GDP-liganded tubulin ring formations have also been reported by others as generally heterogeneous, and contain a mixture of single, double, triple and incomplete rings, as well as spirals. Tubulin ring formations in a solution previously reported are only apparently uniform and some of the ring preparations are heterogeneous, making image-reconstitution studies difficult. For that reason, details about the formation processes of the tubulin ring have not yet been sufficiently sorted out.

In our previous work (*18*), a novel molecular glue which had nine guanidinium groups in a fan shape with dendron scaffold was shown to effectively stabilize the microtubules. In comparing different but coexisting arragements of nine guanidinium groups such as fan-shaped and linear-form, we find a different functional behaviour emerging when using Arg_9 in a straight chain conformation. Although it is beyond the scope of this preliminary study to determine the molecular arrangement and structural analysis in high resolution, we here report the condition under which Arg_9 interacts with α/β tubulin to form a ring with uniformity in size, which crystallizes two-dimensionally in the state.

Although the three-dimensional structure of α/β tubulin in a straight protofilament (microtubule) has been analysed by both cryo-transmission electron microscopy (TEM) and X-ray methods, that of tubulin dimer in the curved protofilament, which can be seen when protofilaments peeling off from the end portion of depolymerizing microtubules, is still unclear. By comparing those in the curved situations during depolymerization and shrinking phase with the current structure in a straight microtubule, one can better understand the fundamental role of tubulin during mitosis and other cellular functions, potentially leading to the development of anti-mitotic drugs, which can disrupt microtubule dynamics.

From the view of nano-biotechnology, the periodic mesoporous structures may attract keen interest from researchers and engineers in nano-fabrication and material science. Experimental results in physiological environment concerning this assembly system are almost non-existent; however this nano-scale construct can serve as a useful structural study for further intermolecular investigations. Another interesting feature of this system is its capacity to form a regular array like two-dimensional crystals. This means, from the viewpoint of material science that there are potential applications in using two-dimensional arrays as the template for building nano-dots array, arranging nano-sized particles, and so forth. This methodology is sufficiently general and not restricted to the originally forming crystalline arrays (*19*).

Materials and Methods

Proteins and reagents

α/β-Tubulin from porcine brain was purchased from Cytoskelton Inc. (Denver, CO, USA). The purity was tested with sodium dodecyl sulphate-polyacrylamide gel electrophoresis (SDS-PAGE) and its capability for spontaneously reconstruction into microtubules was examined by high-performance liquid chromatography (HPLC) gel filtration profiles and TEM according to the manufacturer's protocol. Arginine nonamer trifluoroacetate salt (Arg_9) was purchased from Bachem AG (Bubendorf, Switzerland). GTP and EGTA were purchased from Sigma-Aldrich, and Pipes was from Dojindo Laboratories (Kumamoto).

Two-dimensional crystallization of α/β-tubulin rings

Two-dimensional crystallization of α/β-tubulin rings was achieved as follows: α/β-tubulin (6.56 mg/ml) in 200 µl of 50 mM Pipes, pH 6.9, 1 mM EGTA, 1 mM $MgCl_2$ and 10% glycerol (PEM-G buffer) was used as stock protein solution A. To 4 µl of stock protein solution A, 0.5 µl of 10 mM GTP in PEM-G buffer was added, and the mixture was incubated for 20 min at 37°C. To this solution of 4.5 µl, 1 µl of

1 mM Arg_9 in 20 mM Tris–HCl, pH 7.0 was applied, mixed, and incubated for another 10 min at 37°C. Then it was cooled to 15°C and kept the state for 20 min. The concentration of Arg_9 used was 0.2 mM in final, and we think this was reasonable and sufficient for tubulin of 60 μM in final as a dimer of 110 kDa.

EM and image processing

After 10-fold dilution, aliquots of the solution containing two-dimensional micro-crystals of α/β-tubulin rings were applied onto the specimen grid covered with a thin carbon film, and was negatively stained with 2% uranyl acetate for 40 s. The specimen grids were scanned at low magnification under dark illumination to reduce radiation damage. After adjusting the astigmatism and focusing at adjacent areas, images of the target area were recorded by making use of a slow scan charge-coupled device (CCD) camera (Gatan Retractable Multiscan Camera) under low electron dose conditions at magnifications of 11,500×, 25,000× and 50,000× in a FEI Tecnai F20 electron microscope (FEI Company, the Netherlands) operated at the accelerating voltage of 120 kV. Magnification was calibrated with single crystals of catalase as standard lattice intervals (6.85 nm, 8.75 nm) (*20*). The images were processed with Digital Micrograph (Gatan Inc.) and further followed by the SPIDER image processing system (Health Research Inc., New York) for single particle analysis (*21*). For each TEM image of the desired two-dimensional crystalline arrays recorded, appropriate images of individual α/β-tubulin ring from each set of two-dimensional micro-crystals were selected, isolated, and rotated to maximize correlation. Although it appears difficult to sort the rings (box out from the two-dimensional crystalline arrays), we selected ring units from the second layer (upper layer, that is, far-side from the carbon support film) estimating from the crystalline borders, with the superimposed quarter arc segments from the neighbour rings in the other layer (Fig. 4B and C; the rings are in a two-layer architecture, in face-to-face manner, in the crystals), along with the degree of coverage with a thicker layer of stain. Initial image of a certain ring was used as a reference. In comparison with the reference, each copy of rings boxed out from each series of the two-dimensional crystalline arrays was assessed by asymmetric rotational correlation. Poorly correlated rings were discarded in the next survey. Therefore, the projections of rings boxed out from the upper layer were averaged together with superimposed four quarter arcs of rings from four diagonal neighbours in the lower layer. Next, normalized cross-correlation function between any two pictures was calculated successively by using Fourier transform relationship. Finally, the projection images derived from the α/β-tubulin rings treated as mono-dispersed particles were averaged after rejecting the rings that correlated poorly by using SPIDER/WEB system on an SGI UNIX cluster (*22*).

Results

In EM, two-dimensional micro-crystals of periodic mesoporous assemblies are frequently observed under the desired experimental conditions and sometimes together with reconstituted microtubular structures. Figure 1A shows an EM image of the two-dimensional crystalline arrays of α/β-tubulin rings. They appear to grow during the later incubation at 15°C because no crystalline assemblies are observed in a fraction from the incubation at 37°C. The component as a sole ring is indicated by the arrow *a*, and the reassembled microtubule is shown by the arrow *b*. At first inspection, it is strange to observe how the crystalline arrays can be self-supporting, that is, how rings adhere to one another. As for the lattice of the plane crystal, a closer examination of the TEM images, however, reveals that there are two types in the manner of contacts or association with neighbour rings, giving a square lattice, which will be discussed in detail later. As shown in Fig. 1B, the computed diffraction pattern of the two-dimensional p4g crystal of α/β-tubulin rings corresponding to the boxed area in A supports the layer group *P*4. The *a**- and *b**-axis of the square lattice are indicated. The arrow head at the sixth order along the *b** axis, (*1*, -6) for example corresponds to a spacing of 6.0 nm. Figure 1C shows the Fourier filtered image of the two-dimensional crystals which was derived from the diffraction pattern in B. All the diffraction spots were masked off with Gaussian shaped circular masks and inverse Fourier transformed. According to the scale calibration, the unit cell dimensions are $a = b = 36.9$ nm, and $\gamma = 90°$. We have assigned the unit cell vector directions and lengths in a way such that the real-space image and its Fourier transform are mutually consistent. Taking a close look at one ring in Fig. 1C, the contact with four neighbours is interpreted as an overlap at the four arcs of the ring, and the remaining four neighbours on diagonal positions have no apparent overlap.

In order to obtain an idea for the ring arrangement in the crystalline arrays, single particle analysis was performed for each ring, constituent of the two-dimensional crystalline arrays. Figure 2 shows the galleries of typical α/β-tubulin rings in end-on views selected and isolated from the two-dimensional p4g crystal data sets (*A*–*I*). Each row from A through I corresponds to the individual rings boxed out from two-dimensional crystalline arrays. Most typical six representatives masked off with Gaussian shaped circular masks are shown on each row. The right-most side panels show the averaged projection image for each row: the number of the ring images used for the average projection were 21 for *A*, 25 for *B*, 14 for *C*, 37 for *D*, 53 for *E*, 62 for *F*, 12 for *G*, 35 for *H* and 34 for *I*. Since these images were recorded from the negatively stained TEM specimens, the resolution runs short of identifying the two concentric circular sub-rings in the ring form, but taking a closer look at the arc of the averaged ring there is strong evidence that the ring consists of two concentric sub-rings as seen in Fig. 2 (averaged rings, right-most panels).

Figure 3A shows an averaged projection image created from all of the images ($n = 293$, from *A* through *I* in Fig. 2) of the end-on views of α/β-tubulin rings. The corresponding one superimposed with a contour map is shown as B. Although the contour map presents the outer diameter as 47.7 nm and inner diameter as 30.6 nm, these are values estimated from severe cut-off as to distribution of mass, thus resulted in a thinner radial masses in comparison with averaged values derived from the direct measurements on images shown in the right panels in Fig. 2 (outer diameter as 49.0 nm and inner diameter as 25.4 nm). As is often the case with measurements using negatively stained TEM images due to the permeation of the stain reagent from the protein outer surface into the molecules, the dimensions of the particles tend to appear smaller than real sizes (*23*).

On some occasion, a two-dimensional crystalline sheet bent over itself has been observed with TEM. Figure 4A shows an example of this, where one lies above another domain (see left side of the image). From these twisted sheets, we find evidence that such a ring in the crystalline array form folds up into

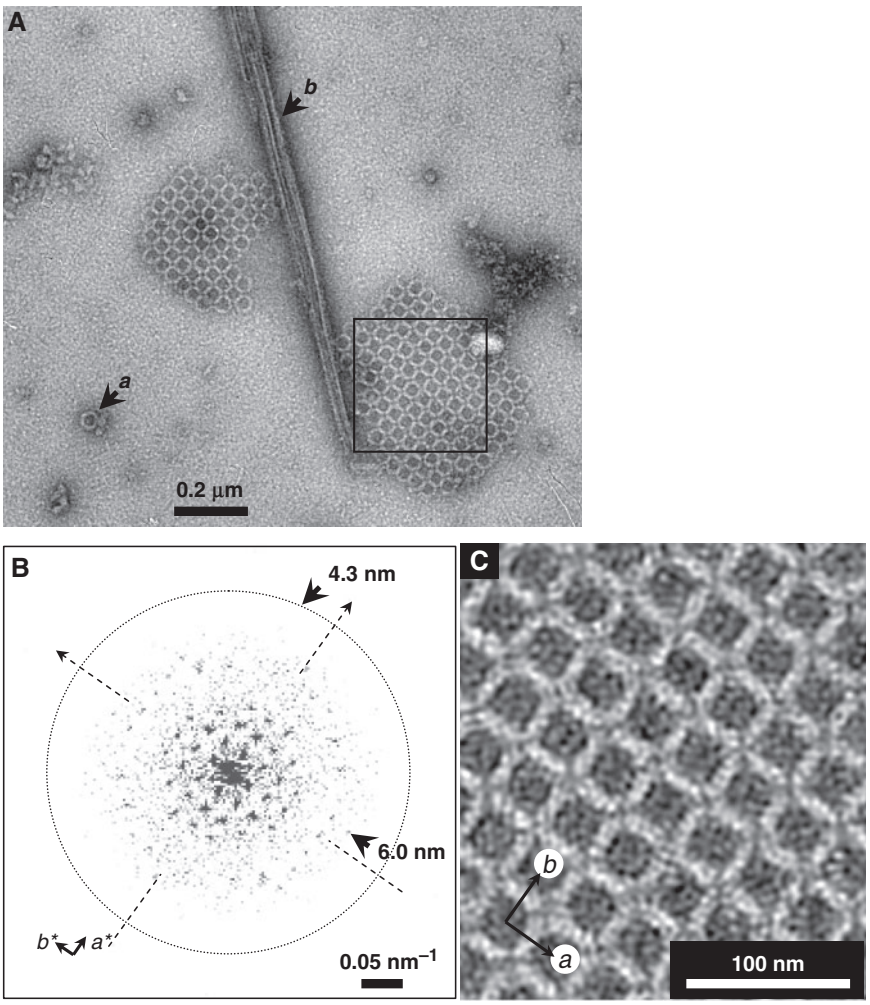

Fig. 1 (A) An electron micrographic image of two-dimensional p4g crystals of α/β-tubulin rings. The two-dimensional crystalline arrays of α/β-tubulin rings appeared to grow during the latter incubation at 15°C. The component as a ring is indicated by the arrow *a*, the reconstituted microtubules by the arrow *b*. Scale bar is 0.2 μm. (B) Computed diffraction pattern of the two-dimensional p4g crystal of α/β-tubulin rings indicated with a box in (A). The *a**- and *b**-axis of the square lattice are indicated. The arrow head at the sixth order along the *b** axis (*1*, -6) corresponds to a spacing of 6.0 nm. Diffraction bar is 0.05 nm^{-1}. (C) Fourier filtered image of two-dimensional crystals showing the diffraction pattern in (B). All the diffraction spots were masked off with Gaussian shaped circular masks and inverse Fourier transformed. $a = b = 36.9$ nm $\gamma = 90°$. Scale bar, 100 nm.

a semi-arc appearance and an understanding of how these ring structures can arrange themselves to form two-dimensional p4g crystals. The depicted schematically is our explanation for the most likely arrangement of α/β-tubulin rings in two-dimensional crystalline arrays. Taking the whole results of the diffraction patterns, the unit cell dimensions, and single particle analysis on each ring isolated from the two-dimensional crystalline arrays into consideration, our model for the two-dimensional crystalline arrays is presented as an end-on direction view of α/β-tubulin ring in Fig. 4B and its side view in C.

Discussion

Although there have been earlier studies on the ring formation of α/β tubulin in various morphologies such as single, double and triple layered rings as well as incomplete rings, they have been generally heterogeneous in sizes. Low-resolution structure modelling in solution of GDP-tubulin double ring was reported by Diaz *et al.* (*24*). They described that the best structure model fit to data is one in which the outer and inner rings have the same polarity such as the parallel double ring model. Nicholson *et al.* (*17*), studied the GDP-liganded tubulin rings formed in the presence of divalent cations and classified different polymer types of double rings into three groups. Those images were averaged by the method for single particle reconstitution. They summarized their results as follows: class 19 (as they mentioned) for 12 α/β-tubulin dimers in the inner ring, 16 dimers in the outer ring, with its inner- and outer- diameter of 30.0 nm and 53.1 nm; class 20 for 11 dimers in the inner ring, 15 dimers in the outer ring, with its inner- and outer-diameter of 23.4 nm and 51.6 nm; class 13 for 10 dimers in the inner ring, 14 dimers in the outer ring, with its inner- and outer-diameter of 17.3 nm and 51.6 nm. The TEM images as for thin crystals of tubulin rings can be seen in the report by Voter and Erickson (*25*).

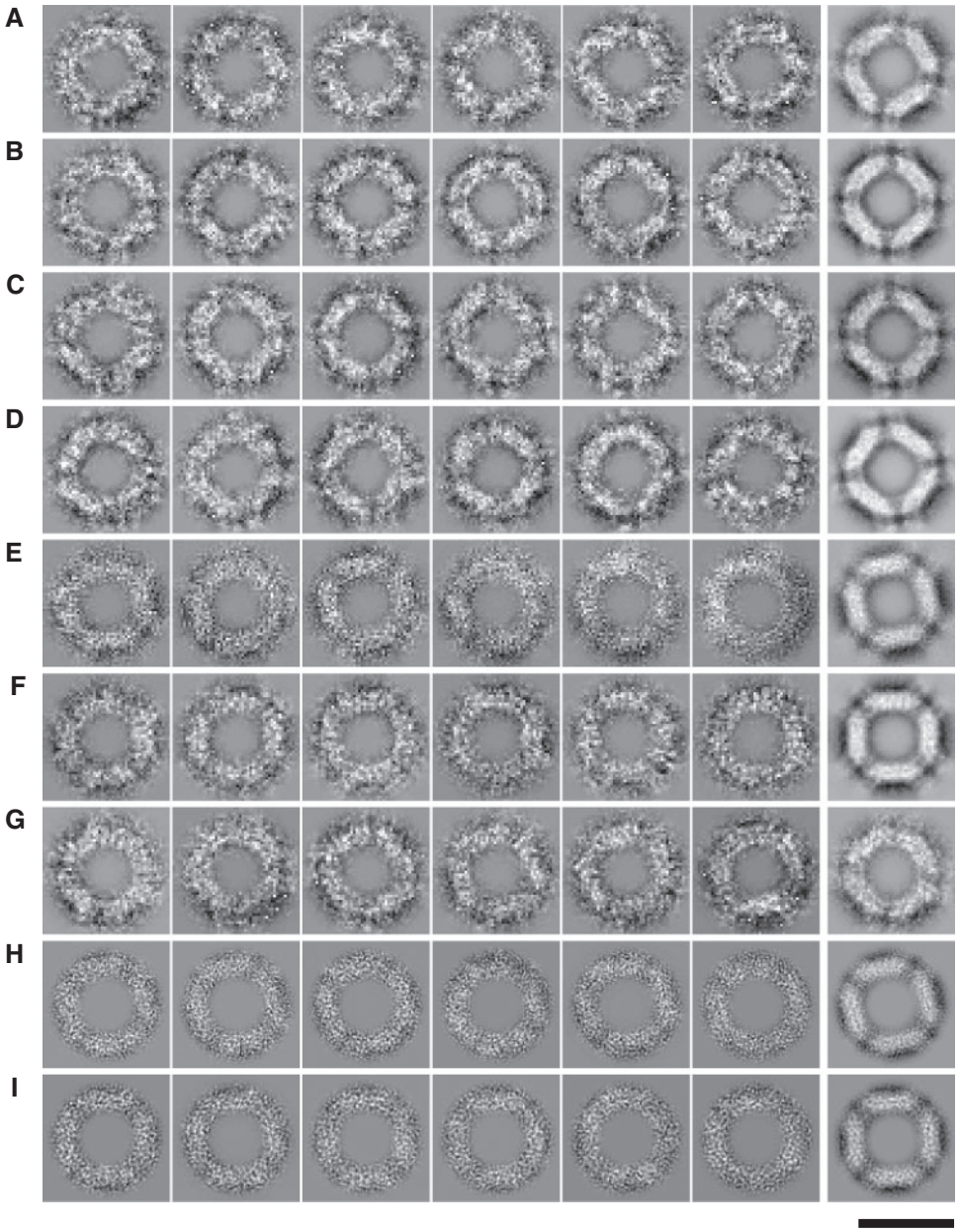

Fig. 2 Isolated images of α/β-tubulin ring in end-on views from each two-dimensional p4g crystal designated as set (*A*–*I*), which were used for single particle image analysis. Rows from *A* through *I* correspond to individual two-dimensional crystalline arrays. Six representatives masked off with Gaussian shaped circular masks are shown on each row. The right-most panels show the averaged projection as for each row: the sum of images used for the averaged projection, *A* ($n = 21$), *B* ($n = 25$), *C* ($n = 14$), *D* ($n = 37$), *E* ($n = 53$), *F* ($n = 62$), *G* ($n = 12$), *H* ($n = 35$) and *I* ($n = 34$). Scale bar, 50 nm.

They concluded that the rings are composed of linear polymers of tubulin subunits equivalent to a protofilament in the microtubule wall in a solely curved conformation. Nevertheless, the low resolution with negative straining, they have made a highly probable speculation on the subunits arrangements in the ring based on the measurements of sizes on a number of different ring structures formed under different conditions. Supposing, the projection of one subunit as 4.0×5.5 nm, their model had 12 dimers in the inner ring, 16 dimers in the outer ring, with its inner- and outer-diameter of 24.0 nm, and 46.0 nm. As shown in Figs 2 and 3, according to our evaluation on ring sizes derived from the real two-dimensional crystalline arrays, the average values of the inner-, and outer-diameters of ring are 25.4 ± 1.1, and 49.0 ± 1.0 nm, respectively. These are comparatively in good agreement with previously reported values. The radial thickness, that is the width of peripheral masses, is calculated as 11.8 ± 1.0 nm from the measured outside and inside diameters. This is consistent with the value in a double ring structure.

In explanation of the poor resolution of the averaged image (Fig. 3), the boxed (isolated) ring image is not a ring from simple single layer. It is a projection of a single ring (consisting of concentric sub-rings) superimposed by four quarter arcs of rings from four diagonal neighbours. This might be major reason for

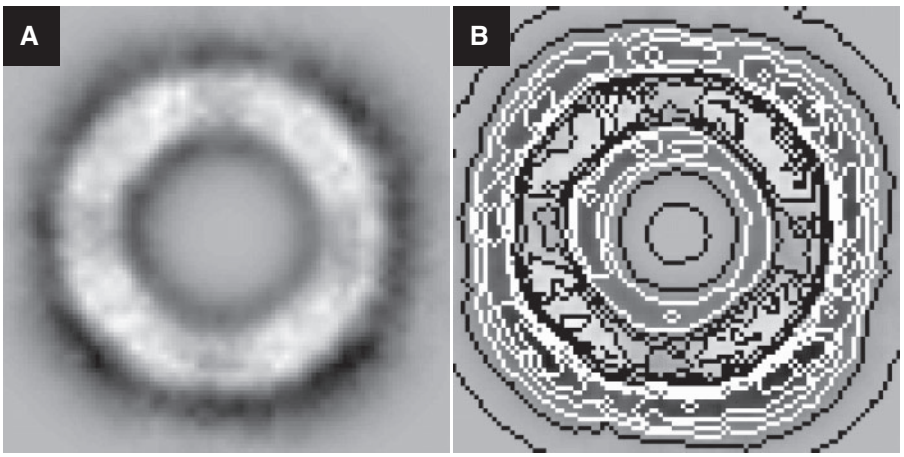

Fig. 3 (A) Averaged projection created from the end-on views (*A* through *I* in Fig. 2) of α/β-tubulin ring ($n = 293$). (B) Corresponding one with contour map. Scale bar, 20 nm. The boxed (isolated) one ring image is not a ring from a simple single layer. It is a projection of a single ring (consisting of concentric sub-rings) superimposed by four quarter arcs of rings from four neighbours. This might be the major reason for the poor resolution in the averaged image along with low resolution due to the negative staining. Since the estimations of the overall dimension are in good agreement with previously reported ones (*17*, *25*), we assume that there are 12 α/β-tubulin dimers in inner ring and 16 dimers in outer ring.

the lack of clarity of the averaged image along with low resolution due to the negative staining. So with the current averaged image at low resolution, it is not clear how many molecules (dimer) reside in each ring (inner- and outer-rings). Yet, estimations of the overall dimension are in good agreement with previously reported ones. Therefore, we assume that there are 12 α/β-tubulin dimers in inner ring and 16 dimers in outer ring.

Although a preliminary X-ray study using the three-dimensional thin crystals of tubulin rings similar to our work was reported by Schönbrunn *et al.* (*26*), their results were hampered by insufficient diffraction data and thus their results fell short of complete structure model determination. In our study, the two-dimensional p4g crystals of α/β-tubulin rings were obtained by adding Arg rather than divalent cations. Most likely the rings are well ordered because the highly acidic C-termini of the tubulin subunits are no longer disordered. This interpretation would reconcile with the findings of Peyrot *et al.* (*27*) that C-terminal cleavage of tubulin by subtilisin enhances ring formation and those of Lobert and Correiat (*28*) who studied crystallization conditions for native and subtilisin-cleaved porcine brain tubulin. The adhesion also takes place by a salt-bridge formation between the guanidinium (Gu^{+}) ions and carboxyl groups that exist ubiquitously in proteins (*29*). It seems worthy to mention that no ring structures were ever seen without Arg_9 under the different experimental conditions as well as even under similar conditions through the study; therefore, Arg_9 may play a role not only in stabilizing the ring structure but also in controlling the uniformity in rings size. However, the detailed mechanisms whereby Arg_9 interact with tubulin and stabilize the ring structures are not known. Further investigation using the two-dimensional p4g crystals of α/β-tubulin rings might be possible to elucidate the location of the C-termini. The role of the C-termini in controlling assembly and aggregation remains a point of great interest.

As shown in Fig. 1, the quality of two-dimensional crystals consisting of α/β-tubulin rings is evaluated by using the diffraction method. Notwithstanding negatively stained two-dimensional crystals, it shows diffraction spots in fairly higher-resolution range. The crystallographic unit cell parameters were calculated to be $a = b = 36.9$ nm and $\gamma = 90^{\circ}$. In the single-particle analysis, as shown in the right-most panels in Fig. 2, four arc overlaps on one ring image are clearly seen. In another words, overlaps of the neighbour rings are emphasized at the four corners in the averaged images. From these analyses, it appears to reconcile some discrepancies between the dimensions of averaged image in end-on views in Figs 2 and 3, and the crystallographic parameters for the two-dimensional crystals. That is, how the component rings are arranged in the two-dimensional crystalline lattice and how it is reconciled with the length of the unit cell vectors in projection. Taking the overlaps at the four corners together with the averaged measurements on the sizes of outer-diameter (49.0 nm) and inner-diameter (25.4 nm) of the ring consisting of two concentric sub-rings (radial thickness of 11.8 nm), the length of the unit vectors *a* and *b* in real space should be around 37.2 nm if the arrangement is assumed Fig. 4B. The error between the lengths of unit vectors both derived from the above calculation and from crystallographic inverse Fourier transform resulted in 0.8%.

This still leaves open the question of whether the two-layer structure is polar or not (*i.e.* do the rings face the same direction or is one layer flipped over relative to the other layer). Never before has crystalline arrays been observed with higher layer thickness for example, 3, 4 or more layers in thickness, and since polar assembly should continue without limit, it seems very likely the two-layer structure is in

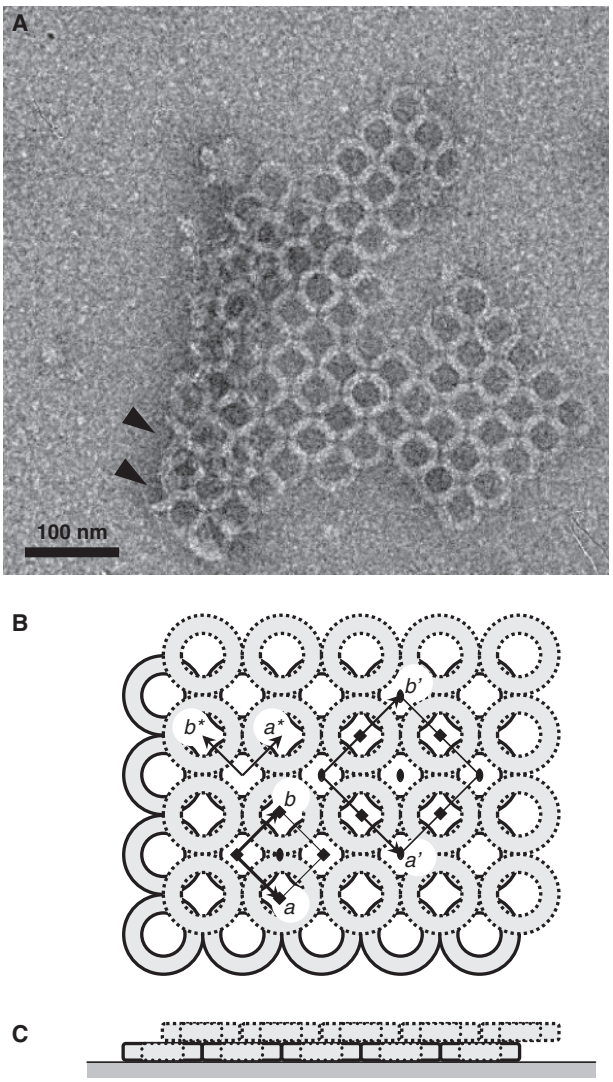

Fig. 4 (A) Electron microscopic image of two-dimensional p4g crystal of α/β-tubulin rings which lies one above another domain (see left side of the image indicated with arrowheads). Scale bar, 100 nm. (B) Explanation of the most probable arrangement of α/β-tubulin rings in two-dimensional crystals. Our model viewed from the end-on direction of α/β-tubulin ring. The vectors *a* and *b* represent apparent unit cell vectors in projection derived from Fourier transform of the projection image of the arrays embedded with negative stain, thus these are not always the unit cell vectors for the three-dimensional crystal structure, composed of two layers in an apolar arrangement. The direction of unit cell vectors *a* and *b* in projection was chosen following Fig. 1 in a way such that real-space image and its Fourier transform are mutually consistent. Strictly from crystallographic views, the unit cell vectors should be *a*′ and *b*′. Crystallographic symmetry elements of the space group $P42_12$ are indicated. (C) Side view of our model.

face-to-face manner. For this reason, non-polar assembly will terminate naturally at the two-layer stage. The primary idea of our speculated model presented is that the two-dimensional p4g crystals are composed of two layered rings, which are overlapped in the manner illustrated in Fig. 4B and C. As shown in Fig. 4A, the EM image of the twisted sheet of the two-dimensional crystals appears to support our idea. Incidentally, strictly from crystallographic views, the unit cell vectors in projection should be *a*′ and *b*′ instead of *a* and *b* as indicated in Fig. 4B. It should be noted that the vectors *a* and *b* drawn in Fig. 4B represent apparent unit cell vectors derived from Fourier transform up to the fifth order diffractions of the projection image by TEM. The diffraction patterns of Fourier transform show that the structure at low resolution (~7.4 nm) has apparent unit cell dimensions $a = b = 36.9$ nm. Thus, these may not be always the unit cell vectors for the real three-dimensional crystal structure, composed of two layers in an apolar arrangement. From the Fourier pattern shown in Fig. 1B, it is conspicuous that the two-dimensional crystals are classified in the layer group *P*4. Examining the results with the TEM images and considering that the two-layer structure is non-polar (layered in face-to-face manner) and the reciprocal lattice symmetry (4/*mmm*), there might be a possibility of the crystals having $P42_12$, supposing the symmetry along *c*-axis which is perpendicular to the crystal plane visible in TEM images. The diffraction of extinction rule at 4*n* might be a reflection of the possible intra-molecular (intra-ring structure) symmetry of heterogeneous domains and/or crystallographic symmetry. The TEM images suggest that the two layers are nearly eclipsed when shifting half the phase mutually along both *a* and *b* axes, even though this is not required by symmetry. The $n = 4$ extinction, corresponding to a spacing about 9.2 nm, would have something to do with the radial thickness, almost equivalent to one fourth of the unit cell length. At very low resolutions, this might be due to the structure being viewed along the *a*- or *b*-axis composed of three layers of non-electron-dense and electron-dense material (domains of the tubulin rings). Further investigations required include the averaging of images of rings having same orientations separated from the other layer, and that three-dimensional reconstruction along with a tilt series of cryo-TEM images of the α/β-tubulin ring two-dimensional crystals derived by Arg_9.

However, details about the formation processes both of the tubulin ring and two-dimensional p4g crystals in the presence of Arg_9 have not been determined. Although determination of detailed molecular arrangement and structural analysis in high resolution are beyond the scope of this preliminary study, the two-dimensional crystalline arrays reported here are useful in the study of molecular packing of α/β tubulin subunits presumably in a different manner which is different from that is seen with zinc sheet, and presents further clues to understanding the molecular dynamics and instability of microtubules.

Chretien *et al.* (*12*) studied inter-protofilament interactions using moiré patterns in cryo-TEM images, and their results show that the flexibility of the microtubules is related to another property of the microtube lattice: the stretching and compressing of the tubulin subunits along the protofilaments. The idea is that the GDP-liganded tubulin rings such like formed in the presence of Arg_9 correspond to unconstrained conformation of GDP-liganded tubulin curving off microtubule ends. Therefore, three-dimensional reconstruction using two-dimensional crystals reported here in combination with tomography method with

cryo-TEM technique of the tubulin rings should be of great interest for understanding dynamic instability of microtubules as well as interactions between the component dimers.

The finding that the ring oligomeric structures consist of the prokaryotic tubulin homolog FtsZ (*30*) indicates that a basic principle of ring assembly is essentially conserved evolutionally, although its physiological function is not understood yet. In general, the property of self-assembly essential for biological macromolecules plays a central role in life. Most of the primary stages of the self-associated architectures involve only the establishment of weak and oriented interactions between homologous molecules. As mentioned earlier, protein tubulin molecules form oligomers and self-associate hierarchically under appropriate conditions. The formation of protein two-dimensional crystals can also be regarded as a prototypical example of molecular self-assembly in the combination with artificial manipulation. In order to engineer protein nano-assemblies using proteins that possess various kinds of physicochemical properties as well as biochemical functions, we need to understand certain features of inter-molecular interactions constituting the driving forces which govern the self-association of protein assemblies, and in the primary stage of two-dimensional crystallization and crystal growth processes. In turn, this understanding can lead to better understanding of the structural diversity of tubulin. Protein molecules reside in different polymeric oligomers, and crystals with their different space groups, may provide a better geometrical understanding of the inter-molecular interactions which can then be exploited by various physical techniques, including the manipulation of molecular orientation of each protein molecule. Using molecular self-assembly, the final structure of the desired protein nano-architectures can be constructed.

When a stretch of amino acids fold into a defined secondary structure motif, these structural prototypes adopt similar structures, but do not necessary have detectable similar conformations. It is estimated that more than a few slightly different conformations may exist in a tubulin molecule from the currently known ones determined by X-ray and electron cryo-crystallography. However, the conformational flexibility of the protein coupled with two-dimensional packing of the rings may be the real difficulty. Reducing the flexibility of the protein structure and improving the order of packing within the crystal may enhance the formation of the two-dimensional p4g crystals. Optimizing the conditions for obtaining larger two-dimensional crystals of the α/β-tubulin rings, along with investigations on how to preserve the flatness of the two-dimensional crystals in TEM imaging are under progress.

Acknowledgements

We would like to express thanks to Prof. R.M. Glaeser, Drs K. Kim and J.L. Mynar for stimulating discussions and critical reading of the manuscript, and Dr K. Hirose for the usage of the TEM facility.

Conflict of interest
None declared.

References

1. Mohri, H. (1968) Amino-acid composition of tubulin constituting microtubules of sperm flagella. *Nature* **217**, 1053–1054
2. Avila, J. (1990) *Microtubule Proteins*. CRC Press, Boca Raton, Florida
3. Löwe, J., Li, H., Downing, K.H., and Nogales, E. (2001) Refined structure of αβ-tubulin at 3.5 Å resolution. *J. Mol. Biol.* **313**, 1045–1057
4. Amos, L.A. and Klug, A. (1974) Arrangement of subunits in flagellar microtubules. *J. Cell Sci.* **14**, 523–549
5. Hyman, A.A. and Karsenti, E. (1996) Morphogenetic properties of microtubules and mitotic spindle assembly. *Cell* **84**, 401–410
6. Nogales, E., Wolf, S.G., and Downing, K.H. (1998) Structure of the alpha beta tubulin dimer by electron crystallography. *Nature* **391**, 199–203
7. Ravelli, R.B.G., Gigant, B., Curmi, P.A., Jourdain, I., Lachkar, S., Sobel, A., and Knossow, M. (2004) Insight into tubulin regulation from a complex with colchicine and a stathmin-like domain. *Nature* **428**, 198–202
8. Mitchison, T. and Kirschner, M. (1984) Dynamic instability of microtubule growth. *Nature* **312**, 237–242
9. Mandelkow, E.-M., Mandelkow, E., and Milligan, R.A. (1991) Microtubules dynamics and microtubules caps: a time-resolved cryo-electron microscopy study. *J. Cell Biol.* **114**, 977–991
10. Nogales, E., Whittaker, M., Milligan, R.A., and Downing, K.H. (1999) High resolution structure of the microtubule. *Cell* **96**, 79–88
11. Wang, H.-E. and Nogales, E. (2005) Nucleotide-dependent bending flexibility of tubulin regulates microtubule assembly. *Nature* **435**, 911–915
12. Chretien, D., Flyvbjerg, H., and Fuller, S.D. (1998) Limited flexibility of the inter-protofilament bonds in microtubules assembled from pure tubulin. *Eur. Biophys. J.* **27**, 490–500
13. Janosi, I.M., Chretien, D., and Flyvbjerg, H. (1998) Modeling elastic properties of microtubule tip and walls. *Eur. Biophys. J.* **27**, 501–513
14. Janosi, I.M., Chretien, D., and Flyvbjerg, H. (2002) Structural microtubule cap: Stability, catastrophe, rescue, and third state. *Biophys. J.* **83**, 1317–1330
15. Vallee, R.B. and Borisy, G.G. (1978) The non-tubulin component of microtubular protein oligomers. *J. Biol. Chem.* **253**, 2834–2845
16. Watts, N.R., Cheng, N., West, W., Steven, A.C., and Sackett, D.L. (2002) The cryptophycin-tubulin ring structure indicates two points of curvature in the tubulin dimer. *Biochemistry* **41**, 12662–12669
17. Nicholson, W.V., Lee, M., Downing, K.H., and Nogales, E. (1999) Cryo-electron microscopy of GDP-tublin rings. *Cell. Biochem. Biophys.* **31**, 175–183
18. Okuro, K., Kinbara, K., Tsumoto, K., Ishii, N., and Aida, T. (2009) Molecular glues carrying multiple guanidinium ion pendants via an oligoether spacer: stabilization of microtubules against depolymerization. *J. Am. Chem. Soc.* **131**, 1626–1627
19. McMillan, R.A., Paavola, C.D., Howard, J., Chan, S., Zaluzec, N.J., and Trent, J.D. (2002) Ordered nanoparticle arrays formed on engineered chaperonin protein templates. *Nat. Mat.* **1**, 247–252
20. Adrian, M., Dubochet, J., Fuller, S.D., and Harris, R. (1998) Cryo-negative staining. *Micron* **29**, 145–160

21. Frank, J., Shimkin, B., and Dowse, H. (1981) Spider—a modular software system for electron image processing. *Ultramicroscopy* **6**, 343–358
22. Frank, J., Radermacher, M., Penczek, P., Zhu, J., Li, Y., Ladjadj, M., and Leith, A. (1996) SPIDER and WEB: Processing and visualization of images in 3D electron microscopy and related fields. *J. Struct. Biol.* **116**, 190–199
23. Harris, J.R. (1997) *Negative Staining and Cryoelectron Microscopy: The Thin Film Techniques*. BIOS Scientific Publishers, Ltd., Oxford, United Kingdom
24. Diaz, J.F., Pantos, E., Bordas, J., and Andreu, J.M. (1994) Solution structure of GDP-tubulin double rings to 3 nm resolution and comparison with microtubules. *J. Mol. Biol.* **238**, 214–225
25. Voter, W.A. and Erickson, H.P. (1979) Tubulin rings: curved filaments with limited flexibility and two modes of association. *J. Suplamol. Struct.* **10**, 419–431
26. Schönbrunn, E., Phlippen, W., Trinczek, B., Sack, S., Eschenburg, S., Mandelkow, E.-M., and Mandelkow, E. (1999) Crystallization of a macromolecular ring assembly of tubulin liganded with the anti-mitotic drug podophyllotoxin. *J. Struct. Biol.* **128**, 211–215
27. Peyrot, V., Briand, C., and Andreu, J.M. (1990) C-terminal cleavage of tubulin by subtilisin enhances ring formation. *Arch. Biochem. Biophys.* **279**, 328–337
28. Lobert, S. and Correiat, J.J. (1991) Studies of crystallization conditions for native and subtilisin-cleaved pig brain tubulin. *Arch. Biochem. Biophys.* **290**, 93–102
29. Schmidtchen, F.P. and Berger, M. (1997) Artificial organic host molecules for anions. *Chem. Rev.* **97**, 1609–1646
30. Erickson, H.P., Taylor, D.W., Taylor, K.A., and Bramhill, D. (1996) Bacterial cell division protein FtsZ assembles into protofilament sheets and minirings, structural homologs of tubulin polymers. *Proc. Natl Acad. Sci. USA* **93**, 519–523